

Prediction of multi-wavelength emissions associated with X-ray flare and extended emission of GRBsRIKI MATSUI ,¹ SHIGEO S. KIMURA ,^{2,1} KOHTA MURASE ,^{3,4,5,6} AND B. THEODORE ZHANG ,^{7,8}¹ *Astronomical Institute, Graduate School of Science, Tohoku University, Sendai 980-8578, Japan*² *Frontier Research Institute for Interdisciplinary Sciences, Tohoku University, Sendai 980-8578, Japan*³ *Department of Astronomy and Astrophysics, The Pennsylvania State University, 525 Davey Laboratory, University Park, PA 16802, USA*⁴ *Institute for Gravitation and the Cosmos, The Pennsylvania State University, University Park, PA 16802, USA*⁵ *Department of Physics; Department of Astronomy & Astrophysics; Center for Multimessenger Astrophysics, Institute for Gravitation and the Cosmos, The Pennsylvania State University, University Park, PA 16802, USA*⁶ *Center for Gravitational Physics and Quantum Information, Yukawa Institute for Theoretical Physics, Kyoto University, Kyoto, Kyoto 606-8502, Japan*⁷ *Key Laboratory of Particle Astrophysics and Experimental Physics Division and Computing Center, Institute of High Energy Physics, Chinese Academy of Sciences, 100049 Beijing, China*⁸ *TIANFU Cosmic Ray Research Center, Chengdu, Sichuan, China***ABSTRACT**

Gamma-ray bursts (GRBs) are one of the most extreme transients in the universe, but their explosion and emission mechanism remains unclear. To investigate the nature of GRB jets, here we focus on X-ray flares (XFs) and extended emissions (EEs), which are X-ray emissions that occur 100 to 1000 seconds after the main burst. They can be observed by recently developed multi-wavelength facilities. In this paper, we calculate emissions across multi-wavelengths associated with XFs and EEs under the hypothesis that XFs and EEs are optically-thin synchrotron emissions from nonthermal electrons in relativistic jets. Considering ranges of the dissipation radius r_{diss} and the Lorentz factor Γ of the jet, we determine the parameter space in which a detectable emission can be produced at each wavelength. We found that simultaneous ultraviolet and very-high-energy gamma-ray emission associated with XFs or EEs can be detected by Swift/UVOT, SVOM/VT, and CTAO approximately every three years. The detection and non-detection rates for each detector are key to determining the uncertain yet essential values necessary for understanding the physics of GRB jets.

Keywords: Gamma-ray bursts (629) — Particle astrophysics (96) — High energy astrophysics (739) —

1. INTRODUCTION

Gamma-ray bursts (GRBs) are one of the most extreme transients in the universe. Their isotropic-equivalent gamma-ray luminosity typically reaches 10^{51} erg/s and such luminous emission is powered by a relativistic jet (W. K. H. Schmidt 1978; B. Paczynski 1986; J. Goodman 1986). The nonthermal spectrum of the burst indicates that nonthermal dissipation within the jet may produce the radiation (D. Band et al. 1993). However, the origin of their jets and gamma-ray emissions remains unresolved.

The main gamma-ray emission of GRBs, the so-called prompt emission, typically lasts around 10 s (C. Kouveliotou et al. 1993). Their prompt emissions require

around ten-seconds reaction time for facilities, which makes difficult to observe at multi-wavelength. This prevents comprehensive multi-wavelength observations and a deeper understanding of the jet, except for a few special events involving prompt-like detections in the optical and GeV bands, such as GRB 080319B (J. L. Racusin et al. 2008), GRB 220101A (Z.-P. Jin et al. 2023), and GRB 221009A (M. Axelsson et al. 2025).

On the other hand, X-ray emission with $\sim 10^{48}$ – 10^{49} erg/s following the prompt phase lasts about 1000 s and appears as either an X-ray flare (XF) or extended emission (EE) (L. Piro et al. 2005; D. N. Burrows et al. 2005a; J. A. Nousek et al. 2006; J. P. Norris & J. T. Bonnell 2006). These types of X-ray emission are observed in about one-third to one-half of all GRBs (T. Sakamoto et al. 2011; C. A. Swenson & P. W. A. Roming 2014; Y. Kaneko et al. 2015; Y. Kagawa et al. 2015, 2019; A. Lien et al. 2016; C. Liu & J. Mao 2019a). They are

roughly 100-1000 times less luminous than the prompt emission, but their integrated energy is comparable (S.-X. Yi et al. 2016; S. Kisaka et al. 2017). Moreover, the short-timescale variability in their light curves is a common feature with the prompt emission (C. A. Swenson et al. 2013; C. A. Swenson & P. W. A. Roming 2014). Although the delay in these emissions indicates that they likely arise from another late jet component⁹ (K. Ioka et al. 2005; R. Perna et al. 2006; B. Zhang et al. 2006a; W.-H. Gao & Y.-Z. Fan 2006; B. D. Metzger et al. 2008; A. Rowlinson et al. 2013; B. P. Gompertz et al. 2014; S. Kisaka & K. Ioka 2015), the dissipation process could be internal dissipation of jets as in the prompt jets (Y. Z. Fan & D. M. Wei 2005; K. Ioka et al. 2005; A. D. Falcone et al. 2006; E. W. Liang et al. 2006; B. Zhang et al. 2006a). The late-time jets that emit XFs and EEs and its dissipation mechanism could be completely different from that of the prompt emission. However, understanding their dissipation should be an important first step in realizing the dissipation process of GRB jets.

In addition to XFs and EEs, ultraviolet (UV) flares are detected with a comparable frequency (C. A. Swenson et al. 2013; S.-X. Yi et al. 2017). Although it is unclear whether UV flares are correlated with XFs or EEs, there are a few flares clearly associated with XFs (S.-X. Yi et al. 2017; R. L. Becerra et al. 2021). These events suggest the possibility of multi-wavelength emission lasting about 1000 s after the main burst of GRBs.

Here, we calculate the broadband emission associated with XFs and EEs, hypothesizing that they are produced by synchrotron radiation from nonthermal electrons in the relativistic jet. Based on this hypothesis, we consistently solve the transport equation while accounting for the full leptonic processes, such as synchrotron emission and self-absorption, inverse Compton scattering, and two-photon ($\gamma\gamma$) absorption. By considering a wide range of dissipation radii r_{diss} and jet Lorentz factors Γ^{10} , we clarify where in the parameter space spectral features of absorption processes can or cannot be detected. Our predictions can be used to constrain the values of r_{diss} and Γ in GRB jets based on future observations. This will lead to a better understanding of the physics of the jets (M. J. Rees & P. Meszaros 1994; M. J. Rees & P. Mészáros 2005; B. Zhang & H. Yan 2011; B.

⁹ The slightly off-axis prompt emission may explain some part of the flares (R. Duque et al. 2022).

¹⁰ Previous studies have constrained the bulk Lorentz factor of jets that produce XFs and EEs (A. D. Falcone et al. 2006; S.-X. Yi et al. 2015; T. Matsumoto et al. 2020), but these constraints are based on the model that each study employs. Here, we seek independent constraints on this parameter.

Zhang & P. Kumar 2013; E. Troja et al. 2015; S.-X. Yi et al. 2015; T. Matsumoto et al. 2020).

This paper is organized as follows. Section 2 presents the method and the setup of our calculations. Section 3 provides the results and the observational expectations. Section 4 discusses an application to a past GRB, the detectability of the flares for the future, a possible contaminated component, and possible extension of this work. Finally, the conclusion is given in Section 5.

Throughout this paper, we use the notation $Q_X = Q/10^X$ in cgs units unless otherwise noted, and denote by Q' the physical quantities in the comoving frame of the jet. We adopt $H_0 = 70 \text{ km s}^{-1} \text{ Mpc}^{-1}$, $\Omega_M = 0.30$, and $\Omega_\Lambda = 0.70$ as cosmological parameters. In addition, in this paper, z and d_L are used as the redshift and the luminosity distance, respectively.

We define the commonly used physical constants as follows: c is the speed of light, σ_T is the Thomson scattering cross section, m_e is the electron mass, m_p is the proton mass, h is the Planck constant, e is the elementary charge.

2. METHOD

Here, we calculate leptonic synchrotron emission for XFs and EEs. Nonthermal synchrotron emission with high radiation efficiency cannot explain the typical broken power-law spectra of prompt emission, especially in the low-energy part (B. Zhang & H. Yan 2011). However, it could be applicable to XFs and EEs, since they are well fitted by a single power law (A. D. Falcone et al. 2007; T. Sakamoto et al. 2011; A. Lien et al. 2016; C. Liu & J. Mao 2019b). Even though some studies for luminous XFs report the broken power-low fitting (A. D. Falcone et al. 2007; F.-K. Peng et al. 2014; C. Liu & J. Mao 2019b)¹¹, the spectral break is unclear for the less luminous, mainly populated XFs and EEs¹². The photon index of the single power-low fitting for typical XFs and EEs is $\sim 1.5\text{-}2$, which is consistent with the synchrotron emission from nonthermal electrons injected with single power-law index $p \sim 2$ (C. D. Dermer & G. Menon 2009) and efficiently cooled by the process.

¹¹ Luminous XFs with luminosities of $\sim 10^{50} \text{ erg/s}$ exhibit a variety of spectral shapes. Some resemble prompt emission, others contain a thermal component, and still others show a single power-law spectrum (F.-K. Peng et al. 2014; C. Liu & J. Mao 2019b; M. Ajello et al. 2019a; Z.-M. Zhou et al. 2025).

¹² Low mass accretion rate $\sim 10^{-3} M_\odot/\text{s}$, required by low-luminosity jets, cannot ignite the neutrino production (W.-H. Lei et al. 2017). The different state of the jet base and the jet composition may involve different dissipation mechanisms and spectral features from those of high-luminosity jets. In this work, we focus on XFs with X-ray luminosities of $\sim 10^{49} \text{ erg/s}$ and assume an electron injection with $p = 2$ for simplicity.

Even if XFs and EEs exhibit broken power-law spectra like prompt emissions, our qualitative picture may still apply.

To estimate the emission spectrum, we adopt a one-zone approximation. The dissipation region is fixed at a radius r_{diss} , where a jet with Lorentz factor Γ dissipates its isotropic luminosity $L_{\text{e,iso}}$ into electrons. We follow a representative fluid element advecting from r_{diss} to $2r_{\text{diss}}$, assuming that its physical quantities represent spatially, directionally, and temporally averaged values within the dissipation region. The momentum-differential number density of electrons $n'_{p'_e}$ and the energy-differential photon number density $n'_{\varepsilon'_\gamma}$ are assumed to be uniform and isotropic. The magnetic field at the dissipation region is also assumed to be uniform.

The following provides a qualitative picture of the radiation process on the comoving frame of the fluid element. The dissipated electrons are continuously injected at a rate $\dot{n}'_{p'_e,\text{diss}}$ and are cooled by adiabatic expansion on a timescale $t'_{\text{dyn}} = r_{\text{diss}}/(c\Gamma)$. The electrons emit synchrotron radiation with an energy-differential and angle-integrated emissivity $j'_{\varepsilon'_\gamma,\text{syn}}$ and are cooled on a timescale t'_{syn} . A fraction of the radiation is absorbed through synchrotron self-absorption (SSA) on a timescale t'_{SSA} or through $\gamma\gamma$ absorption on a timescale $t'_{\gamma\gamma}$. Electrons and positrons are produced by $\gamma\gamma$ interactions at a rate $\dot{n}'_{p'_e,\gamma\gamma}$, and they emit synchrotron radiation again. In addition, Compton scattering redistributes both electrons and photons. We define t'_{ic} as the inverse Compton cooling timescale for electrons, $t'_{\gamma,\text{ic}}$ as the Compton scattering timescale for photons, and $j'_{\varepsilon'_\gamma,\text{ic}}$ as the emissivity of inverse Compton scattering. The photons produced through these processes escape from the emission region on a timescale t'_{esc} . This timescale is defined as the light crossing time of the radial width of the dissipation region $\Delta r'$, therefore, $t'_{\text{esc}} = \Delta r'/c$. Using this t'_{esc} , The observed flux is proportional to $n'_{\varepsilon'_\gamma}/t'_{\text{esc}}$.

We describe the above processes using the transport equations in momentum space (C. D. Dermer & G. Menon 2009):

$$\begin{aligned} \frac{\partial n'_{p'_e}}{\partial t'} - \frac{\partial}{\partial p'_e} \left(\frac{p'_e n'_{p'_e}}{t'_{\text{cool}}} \right) &= \dot{n}'_{p'_e,\text{diss}} + \dot{n}'_{p'_e,\gamma\gamma}, \\ \frac{\partial n'_{\varepsilon'_\gamma}}{\partial t'} &= -\frac{n'_{\varepsilon'_\gamma}}{t'_{\text{dyn}}} - \frac{n'_{\varepsilon'_\gamma}}{t'_{\text{abs}}} + j'_{\varepsilon'_\gamma}, \end{aligned} \quad (1)$$

where t' is the time, p'_e is the momentum of an electron or positron, ε'_γ is the photon energy, $t'_{\text{cool}} = (t'_{\text{syn}}^{-1} + t'_{\text{ic}}^{-1} + t'_{\text{dyn}}^{-1})^{-1}$ is the total cooling timescale, $t'_{\text{abs}} = (t'_{\gamma\gamma}^{-1} + t'_{\text{SSA}}^{-1} + t'_{\gamma,\text{ic}}^{-1})^{-1}$ is the total effective absorption timescale, and $j'_{\varepsilon'_\gamma} = j'_{\varepsilon'_\gamma,\text{syn}} + j'_{\varepsilon'_\gamma,\text{ic}}$ is the total

emissivity. We neglect electron-positron annihilation, SSA heating of electrons, and diffusive heating and cooling by continuous Thomson scattering (I. Vurm & J. Poutanen 2009).

To solve Equations (1), we employ the Astrophysical Multimessenger Emission Simulator (AMES) (B. T. Zhang & K. Murase 2023). AMES includes all the processes in Equation (1), as well as attenuation by the extra-galactic background light (EBL). It provides $n'_{\varepsilon'_\gamma}$ (in units of $\text{erg}^{-1} \text{cm}^{-3}$) from $t' = 0$ to $t' = t'_{\text{dyn}}$. The observed time-averaged flux (in units of $\text{erg cm}^{-2} \text{s}^{-1}$) is then estimated as (C. D. Dermer & G. Menon 2009)

$$\begin{aligned} \varepsilon'_\gamma F_{\varepsilon'_\gamma} &= \frac{r_{\text{diss}}^2 \Delta r' \Gamma^2}{d_L^2} \left\langle \varepsilon'^2 \frac{n'_{\varepsilon'_\gamma}}{t'_{\text{esc}}} \right\rangle \Big|_{\varepsilon'_\gamma = \varepsilon_\gamma(1+z)/\Gamma} \exp[-\tau_{\text{EBL}}(\varepsilon_\gamma)], \\ &= \frac{r_{\text{diss}}^2 c \Gamma^2}{d_L^2} \left\langle \varepsilon'^2 n'_{\varepsilon'_\gamma} \right\rangle \Big|_{\varepsilon'_\gamma = \varepsilon_\gamma(1+z)/\Gamma} \exp[-\tau_{\text{EBL}}(\varepsilon_\gamma)], \end{aligned} \quad (2)$$

where

$$\langle x \rangle = \int_0^{t'_{\text{dyn}}} \frac{dt'}{t'_{\text{dyn}}} x \quad (3)$$

is the average of a value x in the calculation time, and τ_{EBL} is the optical depth of EBL (R. C. Gilmore et al. 2012).

We set following parameters related to the dissipation. As internal dissipation models, the shock between the jet material and the reconnection-driven turbulence are frequently discussed (M. J. Rees & P. Meszaros 1994; B. Zhang & H. Yan 2011), but here we use the formulation that can be applied to both. The nonthermal electron energy densities can be written as $U'_e = L_{\text{e,iso}}/(4\pi r_{\text{diss}}^2 \Gamma^2 c)$, and we set the energy injection rate of the electrons as $\dot{U}'_{\text{e,inj}} = U'_e/t'_{\text{dyn}}$. In addition, magnetic field energy density is set as $U'_B = \xi_B U'_e$ with a parameter ξ_B .

We define $p'_{e,\text{min}}$ and $p'_{e,\text{max}}$ as the minimum and maximum momentum of the injected electrons. Based on these definitions, we assume that the differential injection rate of electrons with respect to the momentum (in units of $\text{cm}^{-3} \text{s}^{-1} (\text{eV}/c)^{-1}$) is given by

$$\dot{n}'_{p'_e,\text{diss}} = C_{\text{norm}} p'_e^{-p} \exp\left(-\frac{p'_e}{p'_{e,\text{max}}}\right) \Theta(p'_e - p'_{e,\text{min}}), \quad (4)$$

where p is the power-law index, Θ is the Heaviside step function, and C_{norm} is a normalization factor. The factor C_{norm} is chosen such that $\int \dot{n}'_{p'_e,\text{diss}} \varepsilon'_e dp'_e = \dot{U}'_{\text{e,inj}}$, where $\varepsilon'_e = \sqrt{p'^2_e c^2 + m_e^2 c^4}$ is the electron energy. Here, $p'_{e,\text{min}}$ is set as a parameter, and $p'_{e,\text{max}}$ is defined such that $t'_{\text{cool}}(p'_{e,\text{max}}) = t'_{\text{acc}}(p'_{e,\text{max}})$, where t'_{acc} is the acceleration timescale of electrons. We assume that the

Table 1. Surveyed parameters

	r_{diss} (cm)	Γ
(A)	3×10^{15}	30
(B)	3×10^{15}	200
(C)	3×10^{15}	500
(a)	10^{14}	80
(b)	10^{14}	200
(c)	10^{14}	500
(E)	10^{13}	150
(F)	10^{13}	500

Table 2. Fixed parameters

$L_{e,\text{iso}}$ (erg/s)	ξ_B	$p'_{e,\text{min}}$ ($m_e c$)	p	d_L (Gpc)	z
10^{50}	10^{-1}	200	2	5.0	0.8

electrons are efficiently accelerated within one cycle of the gyro motion in the dissipation process. The acceleration timescale as a function of p'_e is given by $t'_{\text{acc}}(p'_e) = p'_e/(eB')$, where the magnetic field is $B' = \sqrt{8\pi U'_B}$.

3. RESULT

Here, we calculate the spectra with AMES for the representative points of $(\Gamma, r_{\text{diss}})$, labeled (A) to (E) and (a) to (c) listed in Table 1 and the parameters listed in Table 2. The spectra for (a) to (c) are similar to that of (A) to (C). They are chosen based on the results shown later. The classical picture assumes that Γ and r_{diss} are connected through the relation $\delta t = r_{\text{diss}}/(2\Gamma^2 c)$, where δt is the variability timescale in the light curve. Although $\delta t \sim 100$ s is often adopted for XFs, in this work we explore a broad range of $r_{\text{diss}}/(2\Gamma^2 c)$ to account for the observational and theoretical uncertainties in both δt and the above relation¹³. The Appendixes A and B provide discussions for the magnetized jet case corre-

¹³ Theoretically, the relation $\delta t = r_{\text{diss}}/(2\Gamma^2 c)$ implicitly assumes a shock-dissipation scenario (B. Zhang 2019), whereas reconnection-driven dissipation does not necessarily follow this relation (B. Zhang & H. Yan 2011). Moreover, although δt is often interpreted as the duration of XFs and EEs (~ 100 s) based on the curvature relation discussed in E. W. Liang et al. (2006), it could represent the duration of central engine activity. The time δt that corresponds to $r_{\text{diss}}/(2\Gamma^2 c)$ should be the minimum variability timescale. The light curves of XFs (F.-K. Peng et al. 2014; Z.-M. Zhou et al. 2025) and EEs (T. Sakamoto et al. 2011; Y. Kaneko et al. 2015) suggest that shorter variability may be present. In addition, observationally, the typical XRT count rate for XFs is ~ 100 photons s^{-1} , making variability on timescales shorter than 0.1 s uncertain with current observations.

sponding to $\xi_B = 10$ and for soft electron injection cases with $p = 2.5$, respectively.

Figure 1 show the resultant spectra. The left and right panels are for $F_\nu = F_{\varepsilon_\gamma} h$ in units of $\text{erg cm}^{-2} \text{ s}^{-1} \text{ Hz}^{-1}$ and for $\varepsilon_\gamma F_{\varepsilon_\gamma}$ in units of $\text{erg cm}^{-2} \text{ s}^{-1}$, respectively. The frequency is defined as $\nu = \varepsilon_\gamma/h$. They are all adjusted to have the typical X-ray luminosity of XFs and EEs: $0.3 - 1 \times 10^{49}$ erg/s. For cases (A)–(C) and (a)–(c), the UV (~ 1 eV) emission is detectable by Swift/UVOT (N. Gehrels et al. 2004) and SVOM/VT (J. L. Atteia et al. 2022). The spectra for (D) and (E) show significant breaks at $\lesssim 0.1$ keV ($\sim 10^{16}$ Hz) made by SSA, preventing Swift/UVOT and SVOM/VT from detecting¹⁴. Moreover, for cases (B), (C), (b), (c), and (E), the very-high-energy (VHE) gamma rays (~ 10 GeV) can be detected by CTAO (W. Hofmann & R. Zanin 2023). The highest energy of photons for these cases are determined by the EBL cut off at around 100 GeV. In contrast, the spectra for (A), (a) and (D) exhibit breaks below ~ 1 GeV made by $\gamma\gamma$ absorption, making it difficult to detect in VHE gamma rays. Other VHE gamma ray detectors such as MAGIC (J. Aleksić et al. 2016), H.E.S.S. (F. Aharonian et al. 2006), VERITAS (T. C. Weekes et al. 2002), LHASSO (Z. Cao et al. 2019) cannot detect emissions from all cases because they are sensitive at > 100 GeV. As their representative, the sensitivity of MAGIC is plotted in Figure 1.

The parameter survey results in $r_{\text{diss}} - \Gamma$ plane is shown in Figure 2. For high Γ and large r_{diss} in the orange region, we expect both UV and VHE emissions to be associated with X-rays. In this region, including cases (B), (C), (b) and (c), SSA and $\gamma\gamma$ absorption do not affect the UV band or the VHE gamma rays. For high Γ and small r_{diss} in the purple region, including cases (E), VHE gamma rays can be as luminous as X-rays, while UV emission is absorbed by SSA. For intermediate Γ and large r_{diss} in the blue region, including case (A) and (a), UV emission can avoid SSA and may be associated with the X-rays, whereas VHE gamma rays are still absorbed by $\gamma\gamma$. For intermediate Γ and small r_{diss} in the red region, including case (D), we expect only X-rays, because the UV emission and VHE gamma rays are fully absorbed by SSA and $\gamma\gamma$ processes, respectively.

The black shaded region indicates areas where the spectral index is harder than 1.5. This is inconsistent with that of typical XFs or EEs. In addition, for low

¹⁴ The left bottom panel of Figure 1 shows the spectra for cases (D) and (E) overlapping with the UVOT detection limit. However, the limit shown corresponds to the sensitivity of the UVOT white band. We confirm that the integrated fluxes over the white band are below the UVOT white-band sensitivity.

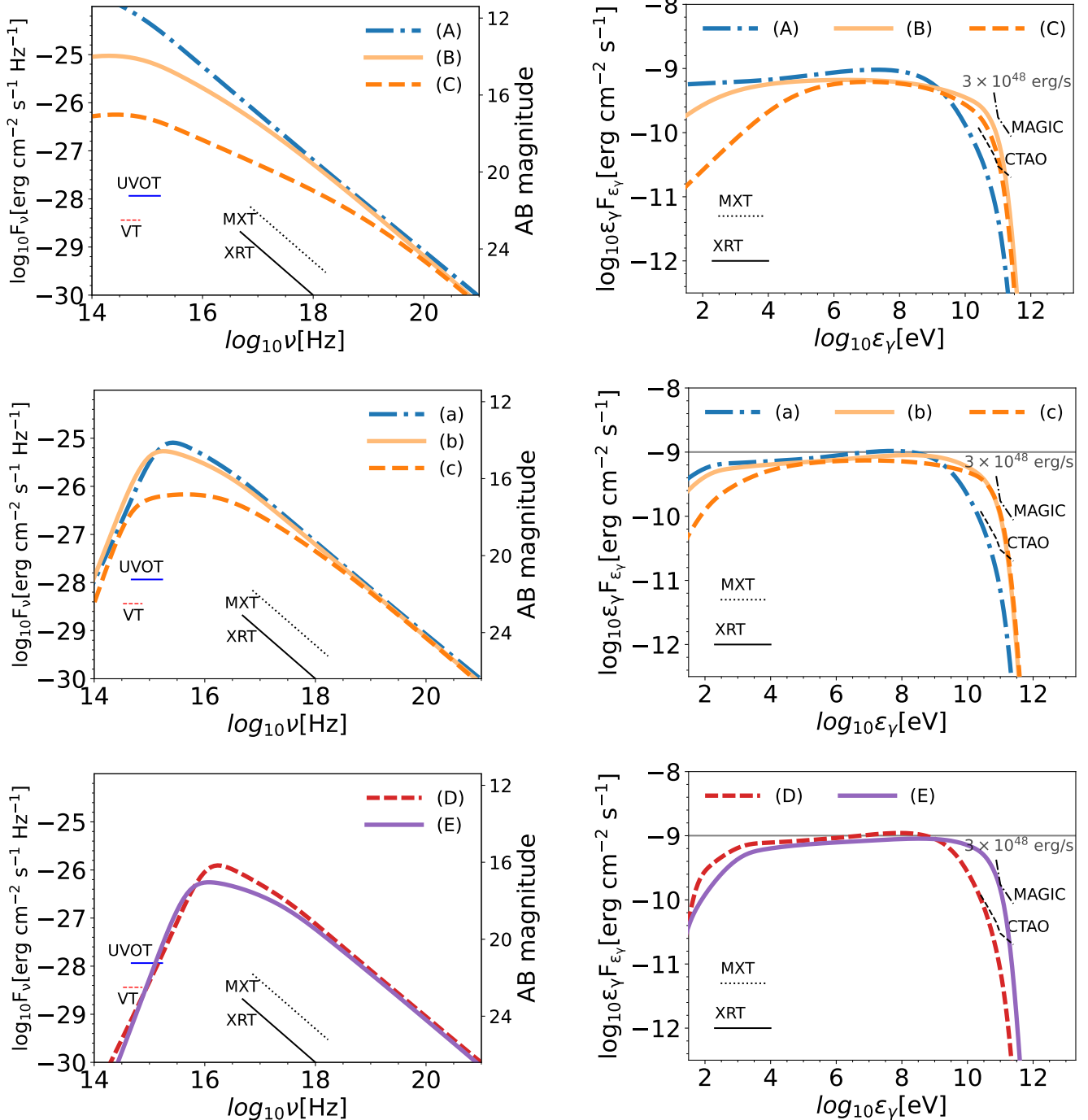


Figure 1. Spectra for cases (A)–(E) and (a)–(c). Right panels is for F_ν , and left panels is for $\nu F_\nu = \varepsilon_\gamma F_{\varepsilon_\gamma}$. The top panels show cases (A)–(C). The dotted-dashed blue line, solid light-orange line, and dashed orange line represent cases (A), (B), and (C), respectively. The middle panels show cases (a)–(c). The dotted-dashed blue line, solid light-orange line, and dashed orange line represent cases (a), (b), and (c), respectively. The bottom panels show cases (D) and (E). The dashed red line, solid purple line correspond to cases (D) and (E), respectively. The horizontal gray lines in right panels ($\varepsilon_\gamma F_{\varepsilon_\gamma}$ plots) indicate the typical luminosity of XFs and EEs, 3×10^{48} erg/s. Thin lines indicate the detection limits for 300-second transients: the dashed red lines are for SVOM/VT (J. L. Atteia et al. 2022), the solid blue lines are for Swift/UVOT (N. Gehrels et al. 2004, 1000 s white sensitivity $\times \sqrt{3}$), the dotted black lines are for SVOM/MXT (J. L. Atteia et al. 2022; D. Gotz et al. 2014), the solid black lines are for Swift/XRT (N. Gehrels et al. 2004; D. N. Burrows et al. 2005b), and the dashed black lines are for CTAO (W. Hofmann & R. Zanin 2023), and the dotted-dashed black lines are for MAGIC (J. Aleksić et al. 2016; V. Fioretti et al. 2019). The CTAO and MAGIC sensitivity lines end at 250 GeV in our plots following Figure 22 in W. Hofmann & R. Zanin (2023) and V. Fioretti et al. (2019), but actually it extends to 100 TeV.

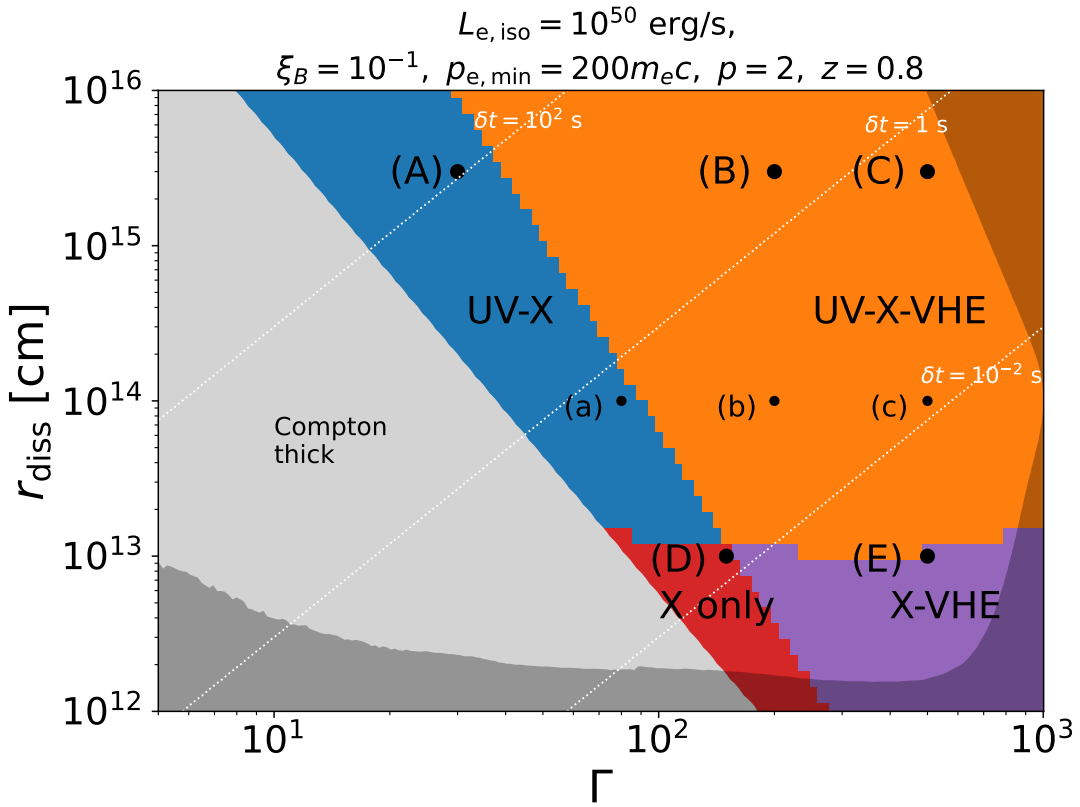


Figure 2. Detectabilities on the r_{diss} - Γ plane. The blue region indicates that UV emission associates with XFs or EEs but no VHE gamma-ray emission. The orange region indicates that both UV (Swift/UVOT) and VHE (CTAO) emissions associate with XFs or EEs. The red region indicates that neither UV nor VHE emission associates with XFs or EEs. The purple region indicates that VHE emission associates with XFs or EEs but no UV emission. The black shaded region is where the photon index at the X-ray band is too hard for the XFs and EEs. The gray region is not considered because the Thomson optical depth exceeds unity and the emission there is subphotospheric. The thin white dotted line represents where the $\delta t = r_{\text{diss}} / (2\Gamma^2 c)$ is constant.

Γ and small r_{diss} in the gray region, the Thomson optical depth, τ_T , exceeds unity (P. Beniamini & P. Kumar 2016). We do not consider the parameter space in this paper. This criterion is equivalent with the limit on the Lorentz factor of EEs given by T. Matsumoto et al. (2020). The photospheric emission in this regime is also discussed in Section 4.4.2.

The MeV gamma-ray luminosity can be comparable to the X-ray luminosity. For a typical luminosity of $\sim 10^{49}$ erg/s and a typical redshift of $z \sim 1\text{--}3$, such emission cannot be detected by Fermi/GBM (M. Axelsson et al. 2025) or Swift/BAT (N. Gehrels et al. 2004) due to their sensitivity limits. However, EEs in MeV gamma rays are detected for some short GRBs (T. Sakamoto et al. 2011; Y. Kaneko et al. 2015). Our fiducial calculation for nearby events such as $z < 0.25$ can explain the observed flux of $\sim 10^{-8}$ erg cm $^{-2}$ s $^{-1}$ at MeV range. If they have comparable GeV flux as cases (B), (C), (b), (c), and (E), Fermi/LAT can detect the event. The Fermi/LAT detectability of such events is discussed in Section 4.

4. DISCUSSION

This section discusses the flares that have actually been observed and expectation of detections for the future. In addition, we discuss theoretically expected extensions of our work at the Section 4.4.

4.1. Case study: GRB 060926

UV flares clearly associated with XFs have been reported for a few GRBs, although comprehensive cross-correlation analyses have not yet been carried out. The light curves presented in S.-X. Yi et al. (2017) for GRB 060926, R. L. Becerra et al. (2021) for GRB 180325A, and Z.-P. Jin et al. (2023) for GRB 220101A show a clear correlation between the X-ray and UV bands.

We focus on GRB 060926 because its flare is comparable in luminosity to a typical X-ray flare, whereas the others are as luminous as the prompt emissions. The parameters chosen for explaining the observation are shown in Table 3, and calculated spectra are shown in Figure 3. The parameters not listed in Table 3 follows Table 2.

Table 3 shows two cases: case 1 and case 2. Case 1 corresponds to a low $\Gamma = 100$, while case 2 corresponds to a high $\Gamma = 1000$. To reproduce the observed UV photons avoiding SSA, both require a relatively large dissipation radius of $r_{\text{diss}} \gtrsim 10^{13}$ cm. At low Γ , the $\gamma\gamma$ absorption has important role, while it is inefficient at high Γ as shown in Figure 2. Thus, VHE gamma-rays $\gtrsim 10$ GeV appear only for case 2. Although it cannot be detected by CTAO due to the suppression by EBL attenuation, the event with the parameter case 2 at

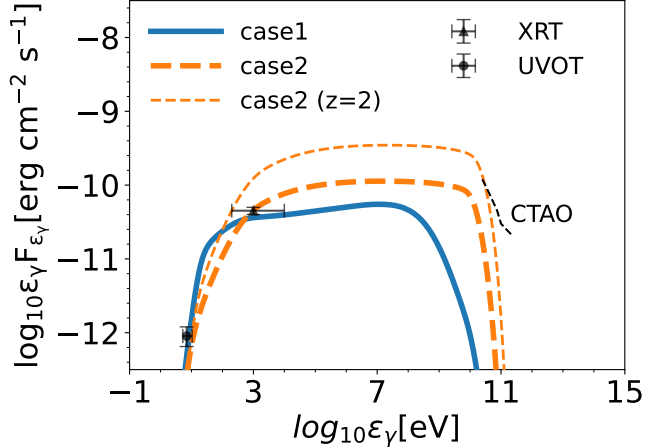


Figure 3. Spectrum of the flare in GRB 060926 at $T - T_0 \sim 10^{2.5}$ s. The thick solid blue line and thick dashed orange line show the spectra for cases 1 and 2 in Table 3, respectively. The thin dashed line shows the spectrum for case 2 at $z = 2$. The triangular and circular points represent the observed data from Swift/XRT and UVOT, respectively. The thin dashed black line indicates the detection limit of CTAO same as in Figure 1 (W. Hofmann & R. Zanin 2023).

Table 3. Parameters for GRB 060926

	$L_{\text{e,iso}}$ (erg/s)	r_{diss} (cm)	Γ	d_L (Gpc)	z
case 1	10^{50}	1.6×10^{13}	10^2	27	3.2
case 2	3×10^{50}	1.6×10^{13}	10^3	27	3.2

$z \lesssim 2$ could be detected by CTAO as shown by the thin dashed line in Figure 3. From this event, we can clearly see that simultaneous observations of the UV and X-ray flares with CTAO are important to constrain the value of Γ .

4.2. Constraint and detection prospects

The UV association for GRB 060926, as discussed in Section 4.1, indicates that r_{diss} exceeds 10^{13} cm for the GRB. However, to analyze the majority of GRBs with flares, we need to examine the cross-correlation between UV and X-ray flares. Since UV flares are reported in 10–30% of long GRBs (C. A. Swenson et al. 2013; C. A. Swenson & P. W. A. Roming 2014; S.-X. Yi et al. 2016, 2017), the cross-correlation analysis is important for understanding the XFs and EEs.

The survey of VHE gamma-ray flares is important to constrain Γ . To observe a GRB with CTAO, an alert localization of ~ 1 degree is required (W. Hofmann & R. Zanin 2023). This means that the GRB must be triggered by Swift/BAT (N. Gehrels et al. 2004) or SVOM/ECLAIR (J. L. Atteia et al. 2022) in

the current situation. The detection rate of GRBs by Swift/BAT is roughly 80 yr^{-1} (A. Lien et al. 2016), and SVOM/ECLAIR is expected to achieve a similar frequency (J. L. Atteia et al. 2022). Additionally, as shown in the right panel of Figure 1, $z \sim 0.8$ represents the detection horizon of VHE gamma rays for CTAO for the flare with typical X-ray luminosity $\sim 10^{49} \text{ erg/s}$. Among the events with measured redshifts, about $\sim 10\%$ are from $z < 0.8$ (A. Lien et al. 2016; J.-M. Hao et al. 2020). From the above arguments, we expect about $\sim 8 \text{ yr}^{-1}$ of $z < 0.8$ GRBs to be detected by Swift/BAT or SVOM/ECLAIR. Considering that 30% of GRBs have XFs or EEs, BAT and ECLAIR can detect about $\sim 3 \text{ yr}^{-1}$ of $z < 0.8$ GRBs with flares. Assuming that roughly 10% of GRBs can be observed by CTAO with a good condition (S. Inoue et al. 2013), a VHE flare can be detected about once every ~ 3 years with current detector systems. Such a detection with CTAO would reveal the Lorentz factor of the flaring jet.

VHE gamma-ray detectors currently conducting GRB follow-up campaigns, such as MAGIC (J. Aleksić et al. 2016), H.E.S.S. (F. Aharonian et al. 2006), VERITAS (T. C. Weekes et al. 2002), and CTA LST-1 (H. Abe et al. 2023), can potentially detect emission associated with XFs and EEs. To constrain $\Gamma \sim 100$, GRBs with redshift $z \lesssim 0.5$ are required to avoid significant attenuation by the EBL. The event rate for $z \lesssim 0.5$ is $\sim 3\text{--}5\%$ of all GRBs (J.-M. Hao et al. 2020). Considering that XFs or EEs are associated with $\sim 30\%$ of GRBs, we expect $\sim 1\text{--}2$ XFs or EEs from $z < 0.5$ per 100 GRBs without redshift measurements. Since these facilities have collectively observed more than 100 GRBs with delays shorter than 1000 s after the prompt emission (S. Abe et al. 2025; D. Ribeiro 2023; B. Cornejo Avila et al. 2026), such observations might already provide meaningful constraints. A careful analysis of the upper limits, particularly accounting for the timing of XFs and EEs, is required.

For nearby events, Fermi/GBM and Fermi/LAT can detect MeV and GeV gamma rays from XFs and EEs. If MeV gamma rays are detected with XFs, it is difficult to distinguish between hundred-second-long prompt emission and XFs based on the light curve alone. On the other hand, EEs may be distinguished from prompt emission in the light curve. For this reason, here we focus on the detection rate of EEs in MeV and GeV gamma rays. According to Y. Kaneko et al. (2015), Fermi/GBM and Swift/BAT detected 28 EE events with fluxes of $\gtrsim 10^{-8} \text{ erg cm}^{-2} \text{ s}^{-1}$ over ~ 8 years. This flux is close to the minimum value observed by LAT in the 100–1000 s interval after the prompt emission of short GRBs (M. Ajello et al. 2019b). This implies that EEs

detectable by Fermi/LAT at $\sim 1 \text{ GeV}$ occur at a rate of $\sim 3.5 \text{ yr}^{-1}$ for the orange and purple regions in Figure 2. Since Fermi/LAT covers about one-sixth of the sky (M. Ajello et al. 2019b), it can detect EEs at a rate of $\sim 0.6 \text{ yr}^{-1}$, which is similar to the expected detection rate of flares by CTAO.

Actually, GeV gamma rays have been detected by Fermi/LAT from several short GRBs over ~ 10 years of observations (M. Ajello et al. 2019b), although it remains unclear whether these emissions are associated with EEs. We do not model them here because redshifts are not determined for most of the events, and the one event with a known redshift shows a light curve that is clearly different from typical EEs. Above arguments demonstrate that Fermi/LAT observations and event by event broadband modelings are also important for constraining the $r_{\text{diss}}\text{-}\Gamma$ plane.

In the near future, nanosatellite constellations such as CAMEROT (N. Werner et al. 2018) and HERMES (F. Fuschino et al. 2019) will improve the detection frequency of events with localization accuracy of about 1 degree. This will increase the chance for CTAO to detect emissions associated with XFs and EEs by a factor of ~ 3 . Therefore, VHE flares could be observed at a rate of $\sim 1 \text{ yr}^{-1}$ with these detectors.

4.3. External inverse Compton at the forward shock

The VHE gamma-ray emission expected in this paper may be contaminated by an emission component from the forward shock (FS), which produces the afterglow. XFs and EEs inevitably provide X-rays that serve as seed photons for external inverse Compton (EIC) scattering at the FS (K. Murase et al. 2011; B. T. Zhang et al. 2021). The resulting EIC emission can reach GeV–TeV energies with energetics comparable to those of XFs and EEs, and it appears at a similar epoch (K. Murase et al. 2011). However, the EIC light curve rises with a time delay of $R_{\text{FS}}/(2c\Gamma_{\text{FS}}^2) > r_{\text{diss}}/(2c\Gamma^2)$ relative to the X-ray flare, where R_{FS} and Γ_{FS} are the radius and Lorentz factor of the FS (A. M. Beloborodov et al. 2014). In addition, the tail of the EIC light curve becomes broader than that of the seed photons due to high-latitude emission (A. M. Beloborodov et al. 2014). In contrast, the VHE gamma rays from our scenario should closely follow the X-ray light curve. Although a fully consistent light-curve calculation is beyond the scope of this work, these two components can, in principle, be distinguished by comparison of VHE light curves with X-ray ones.

4.4. Possible extension

In this work, we ignore the contribution from following components shown in this subsection. It is possible to extend our work to include them.

4.4.1. Hadronic emission associated with X-ray flares and extended emission

The dissipation could accelerate protons or heavier nuclei in the jet (E. Waxman 1995; M. Vietri 1995). These dissipated hadrons can emit gamma rays through inelastic nuclei-photon collisions ($p\gamma$ process for protons) and nuclei-nuclei collision (pp process for protons) (E. Waxman & J. Bahcall 1997; M. Böttcher & C. D. Dermer 1998; K. Asano & S. Inoue 2007; K. Asano et al. 2009; K. Murase et al. 2012). Spectral calculations with dissipated hadrons are beyond the scope of this discussion. However, our calculations may mimic the hadronic results for the following reasons: First, the photons from the hadronic process are high energy, greater than or equal to 1 GeV, at the jet rest frame. These photons are easily absorbed by low-energy photons, creating copious electron-positron pairs. These pairs produce synchrotron emissions. This cascading process converts the jet energy into leptonic energy. This may lead to similar energetics as a purely leptonic process, although the spectra should be modified (K. Asano & S. Inoue 2007; K. Asano et al. 2009; K. Murase et al. 2012). Alternatively, if the Lorentz factor is very large, cascades become less efficient, in which nuclear synchrotron emission or secondaries from the Bethe-Heitler process can be relevant (K. Murase & J. F. Beacom 2010).

High-energy neutrino observations provide another way to constrain the $r_{\text{diss}}-\Gamma$ plane. For low $\Gamma < 100$ in the blue and red regions of Figure 2, photons produced within the dissipation region can participate in the $p\gamma$ process, leading to neutrino production in the TeV–PeV energy range (K. Murase & S. Nagataki 2006). If XFs and EEs are from photosphere (see Section 4.4.2), not only $p\gamma$ interactions but also pp interactions can also be relevant (K. Murase 2008).

For high $\Gamma > 100$ with small $r_{\text{diss}} < 10^{13}$ cm in the purple region of Figure 2, external photons from the cocoon (see Section 4.4.3) may enhance the $p\gamma$ process (R. Matsui et al. 2023, 2024). Meanwhile, the cocoon photons may kill VHE photons through $\gamma\gamma$ absorption. A fully consistent numerical calculation and parameter survey covering these multi-messenger signals is left for future work.

4.4.2. Photospheric emission

XFs and EEs can originate from the photosphere, gray region in Figure 2. Inside the photosphere, nonther-

mal dissipation become not simple because of mediation by radiation (J. Zrake et al. 2019; C. Lundman & A. M. Beloborodov 2019a,b). Further study is needed to explain XFs and EEs through subphotospheric dissipation that includes full electromagnetic processes and hydrodynamics (I. Vurm & J. Poutanen 2009; A. M. Beloborodov 2017; C. Lundman & A. M. Beloborodov 2019a; J. Zrake et al. 2019). Moreover, SSA and Compton heating of electrons and electron-positron annihilation could affect the photon spectra in the gray region (I. Vurm & J. Poutanen 2009). Calculations with all these processes are left for future work.

4.4.3. Cocoon

The interaction between the prompt jet and the progenitor star forms the structure called “cocoon” (P. Mészáros & M. J. Rees 2001; C. D. Matzner 2003; O. Bromberg et al. 2011; E. Nakar & T. Piran 2017; O. Gottlieb et al. 2020, 2021; H. Hamidani & K. Ioka 2021). The cocoon expands after the jet breakout (H. Hamidani & K. Ioka 2023). The expanded cocoon component can affect the emission of multi-wavelength flares or EEs.

If r_{diss} lies within the cocoon radius, external photons from the cocoon can enter the dissipation region and serve as seed photons for inverse Compton emission and $p\gamma$ process (K. Toma et al. 2009; S. S. Kimura et al. 2019; A. Mei et al. 2022; R. Matsui et al. 2023, 2024).

The cocoon effect is typically significant for $r_{\text{diss}} < 10^{13}$ cm and $\Gamma > 200$, roughly overlapping with the purple region in Figure 2 (R. Matsui et al. 2023, 2024). However, the cocoon energy strongly depends on the luminosity and magnetic field of the prompt jet (E. Nakar & T. Piran 2017; O. Gottlieb et al. 2020, 2021; H. Hamidani & K. Ioka 2023), and the strength of the effect depends on the time after the main burst (S. S. Kimura et al. 2019; R. Matsui et al. 2023, 2024), which reduces the simplicity of the picture. This effect needs to be considered on an event-by-event basis. A detailed calculation including the cocoon effect is beyond the scope of this work.

4.4.4. Shallow-decay phase and plateau emission

The shallow-decay phase in long GRBs and the plateau emission in short GRBs are X-ray components characterized by relatively flat light curves (e.g., J. A. Nousek et al. 2006; S. Kisaka et al. 2017). The shallow-decay phase appears at $\sim 10^3$ – 10^4 s after the prompt emission with a luminosity of $\sim 10^{46}$ – 10^{48} erg/s (J. A. Nousek et al. 2006; B. Zhang et al. 2006b; M. G. Dainotti et al. 2010; M. G. Bernardini et al. 2012), whereas the plateau emission appears at $\sim 10^4$ – 10^5 s with a luminosity of $\sim 10^{45}$ – 10^{47} erg/s (B. P. Gompertz et al. 2013;

S. Kisaka et al. 2017). Their origins are still under debate, but they could arise from internal dissipation of late jet components (P. Kumar et al. 2008; G. Ghisellini et al. 2009; N. Lyons et al. 2010), although the variability properties of their light curves remain unclear. Therefore, the discussion in this paper may also be applicable to these components.

However, the X-ray luminosities of these components are lower than those of XFs and EEs. Since the UV and VHE gamma-ray luminosities are expected to be comparable to the X-ray luminosity at maximum, detecting them from $z \gtrsim 1$ is challenging based on our model. Therefore, we must wait for nearby events to detect broadband emission associated with these components.

5. CONCLUSION

We calculate the multi-wavelength flux associated with XFs and EEs over a broad range r_{diss} and Γ in Table 1, using the parameters listed in Table 2. The spectra shown in Figure 1 suggest the possible simultaneous detection of UV, X-ray, and VHE gamma-ray emission 100–1000 s after the prompt emission of GRBs, associated with XFs or EEs. In particular, the VHE gamma-rays are expected to be observed once a ~ 3 years by CTAO, assuming the 10% of its duty cycle and considering that $\sim 30\%$ of GRBs have flares. Addition-

ally, Figure 2 indicates where in the $r_{\text{diss}}\text{-}\Gamma$ plane the UV to VHE gamma rays can be detected by Swift/UVOT and CTAO. According to the Figure 2, the detection of UV suggests $r_{\text{diss}} > 10^{13}$ cm, while the VHE gamma-ray detection does $\Gamma > 100$. The actual detection and non-detection rates of multi-wavelength emission are important for constraining the uncertain yet essential parameters r_{diss} and Γ , which are key to understanding the physics of relativistic jets. Future surveys of flares by Swift, SVOM, and CTAO may reveal these values.

ACKNOWLEDGMENTS

The authors thank Yuri Sato for meaningful discussions. This work is supported by Graduate Program on Physics for the Universe (GP-PU), and JSPS KAKENHI Nos. 25KJ0587 (R.M.) 22K14028, 21H04487, and 23H04899 (S.S.K.). S.S.K. acknowledges the support by the Tohoku Initiative for Fostering Global Researchers for Interdisciplinary Sciences (TI-FRIS) of MEXT’s Strategic Professional Development Program for Young Researchers. The work of K.M. was supported by the NSF Grants No. AST-2108466, No. AST-2108467, and No. 2308021, and KAKENHI No. 20H05852. B.T.Z. is supported in China by National Key R&D program of China under the grant 2024YFA1611402.

APPENDIX

A. MAGNETIZED JET CASE

In the main text, we discuss the dissipation of an unmagnetized jet in the limit $\xi_B < 1$, but it is also possible that magnetic field energy dominates the jet prior to dissipation. Such a magnetized jet may dissipate its energy into electrons as it approaches equipartition. To account for this limit, we adopt $\xi_B = 1$.

Figure 4 shows the detectability in the $r_{\text{diss}}\text{-}\Gamma$ plane for the magnetized jet case. For these cases, the synchrotron burn-off limit around $\sim 8 \Gamma_2[(1+z)/2]^{-1}$ GeV become significant. This produces an exponential cutoff above that energy. This cutoff prevents us from detecting VHE gamma rays by CTAO for $\Gamma \sim 50\text{--}200$, which is the most significant difference comparing to the case with $\xi_B = 10^{-1}$.

B. SOFT ELECTRON INJECTION CASE

In the main text, we assume an electron injection with $p = 2$, which results in hard spectra for both electrons and photons. However, this value of p is theoretically and observationally uncertain. Here, we examine cases

with $p = 2.5$ as a representative soft injection limit for XFs and EEs. Figure 5 shows the spectra for $p = 2.5$ with the same parameters as in Tables 1 and 2. A two-hump structure is visible in all spectra except for the case (C), produced by the primary synchrotron and its self-inverse Compton (SSC) components. The SSC component is responsible for the detectability of VHE gamma rays.

Overall, the detectability is similar to that for $p = 2$, but the spectra for the case (C) do not reach the CTAO sensitivity. This is because the case is in the slow-cooling regime, where the radiation efficiency is lower than 100%. The SSC component is suppressed as the primary synchrotron emissions, or seed photons, decrease.

Figure 6 shows the detectability in the $r_{\text{diss}}\text{-}\Gamma$ plane for the soft injection ($p = 2.5$). The detectability of VHE gamma rays are modified for around the case (C), high $\Gamma > 300\text{--}500$ and large $r_{\text{diss}} > 10^{14}\text{--}10^{16}$ cm. Figure 7 shows the detectability in the $r_{\text{diss}}\text{-}\Gamma$ plane for soft injection and magnetized jet case ($p = 2.5$ and $\xi_B = 10$). Since the inverse-Compton emission is inefficient

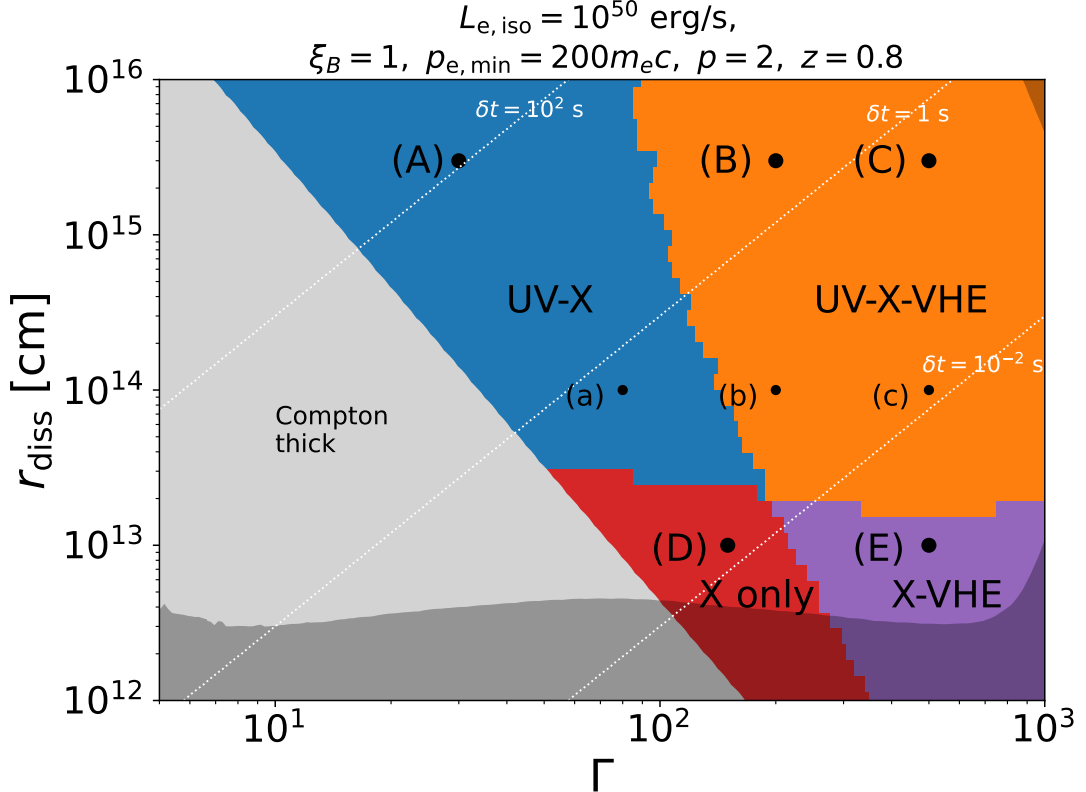


Figure 4. Same as Figure 2 but for the magnetized jet.

for $\xi_B = 1$, the parameter space where the VHE gamma rays can be detected become narrow. These plots make the complexity for constraining the $r_{\text{diss}}-\Gamma$ plane. We

need to clarify the value of p from observed spectra when we constrain the $r_{\text{diss}}-\Gamma$.

REFERENCES

Abe, H., Abe, K., Abe, S., et al. 2023, ApJ, 956, 80, doi: [10.3847/1538-4357/ace89d](https://doi.org/10.3847/1538-4357/ace89d)

Abe, S., Abhir, J., Abhishek, A., et al. 2025, A&A, 700, A96, doi: [10.1051/0004-6361/202555468](https://doi.org/10.1051/0004-6361/202555468)

Aharonian, F., Akhperjanian, A. G., Bazer-Bachi, A. R., et al. 2006, A&A, 457, 899, doi: [10.1051/0004-6361:20065351](https://doi.org/10.1051/0004-6361:20065351)

Ajello, M., Arimoto, M., Asano, K., et al. 2019a, ApJL, 886, L33, doi: [10.3847/2041-8213/ab564f](https://doi.org/10.3847/2041-8213/ab564f)

Ajello, M., Arimoto, M., Axelsson, M., et al. 2019b, ApJ, 878, 52, doi: [10.3847/1538-4357/ab1d4e](https://doi.org/10.3847/1538-4357/ab1d4e)

Aleksić, J., Ansoldi, S., Antonelli, L. A., et al. 2016, Astroparticle Physics, 72, 76, doi: [10.1016/j.astropartphys.2015.02.005](https://doi.org/10.1016/j.astropartphys.2015.02.005)

Asano, K., & Inoue, S. 2007, ApJ, 671, 645, doi: [10.1086/522939](https://doi.org/10.1086/522939)

Asano, K., Inoue, S., & Mészáros, P. 2009, ApJ, 699, 953, doi: [10.1088/0004-637X/699/2/953](https://doi.org/10.1088/0004-637X/699/2/953)

Atteia, J. L., Cordier, B., & Wei, J. 2022, International Journal of Modern Physics D, 31, 2230008, doi: [10.1142/S0218271822300087](https://doi.org/10.1142/S0218271822300087)

Axelsson, M., Ajello, M., Arimoto, M., et al. 2025, ApJS, 277, 24, doi: [10.3847/1538-4365/ada272](https://doi.org/10.3847/1538-4365/ada272)

Band, D., Matteson, J., Ford, L., et al. 1993, ApJ, 413, 281, doi: [10.1086/172995](https://doi.org/10.1086/172995)

Becerra, R. L., De Colle, F., Cantó, J., et al. 2021, ApJ, 908, 39, doi: [10.3847/1538-4357/abcd3a](https://doi.org/10.3847/1538-4357/abcd3a)

Beloborodov, A. M. 2017, ApJ, 838, 125, doi: [10.3847/1538-4357/aa5c8c](https://doi.org/10.3847/1538-4357/aa5c8c)

Beloborodov, A. M., Hascoët, R., & Vurm, I. 2014, ApJ, 788, 36, doi: [10.1088/0004-637X/788/1/36](https://doi.org/10.1088/0004-637X/788/1/36)

Beniamini, P., & Kumar, P. 2016, MNRAS, 457, L108, doi: [10.1093/mnrasl/slw003](https://doi.org/10.1093/mnrasl/slw003)

Bernardini, M. G., Margutti, R., Mao, J., Zaninoni, E., & Chincarini, G. 2012, A&A, 539, A3, doi: [10.1051/0004-6361/201117895](https://doi.org/10.1051/0004-6361/201117895)

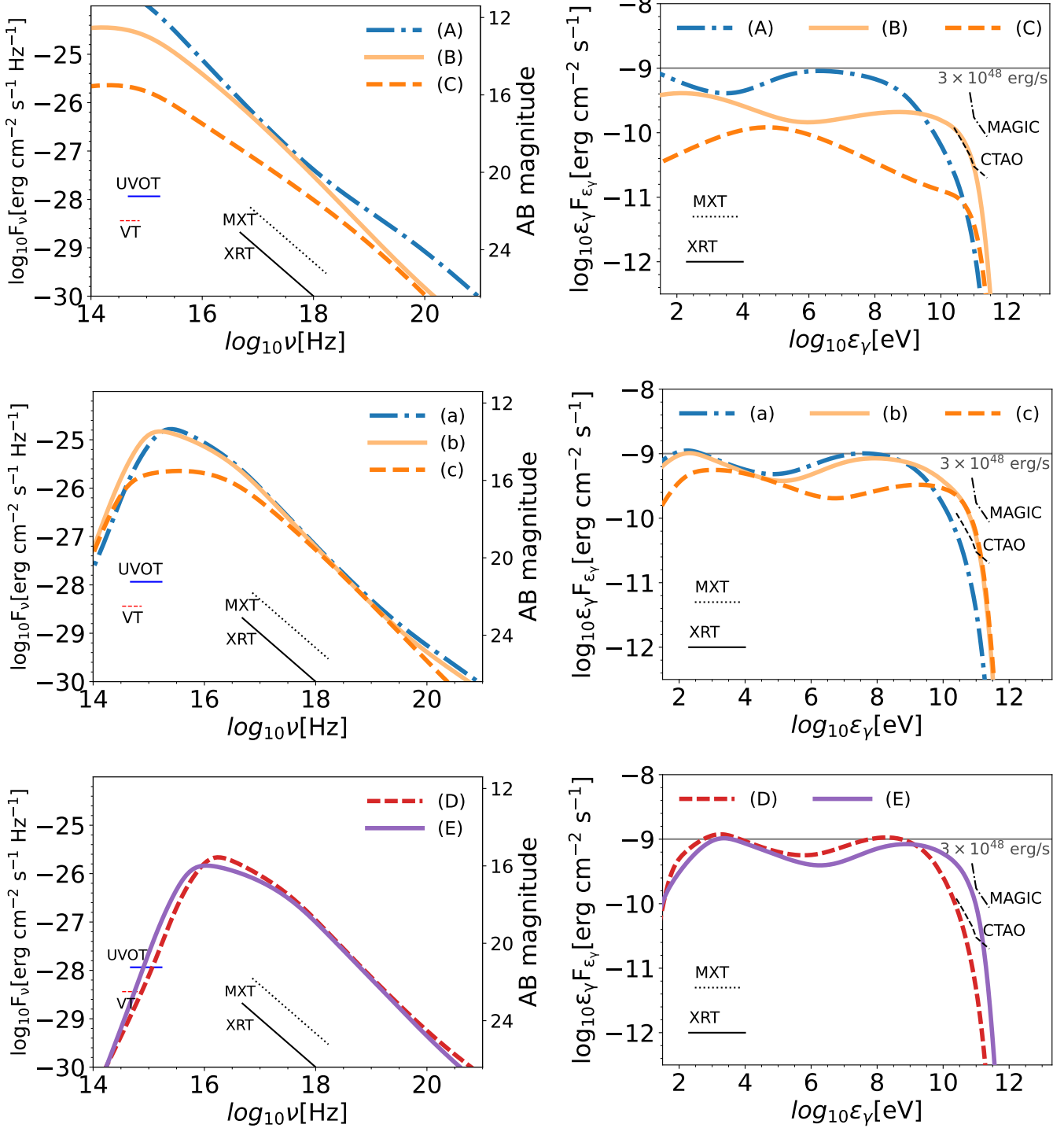


Figure 5. Same as Figure 1 but for the soft electron injection case ($p = 2.5$).

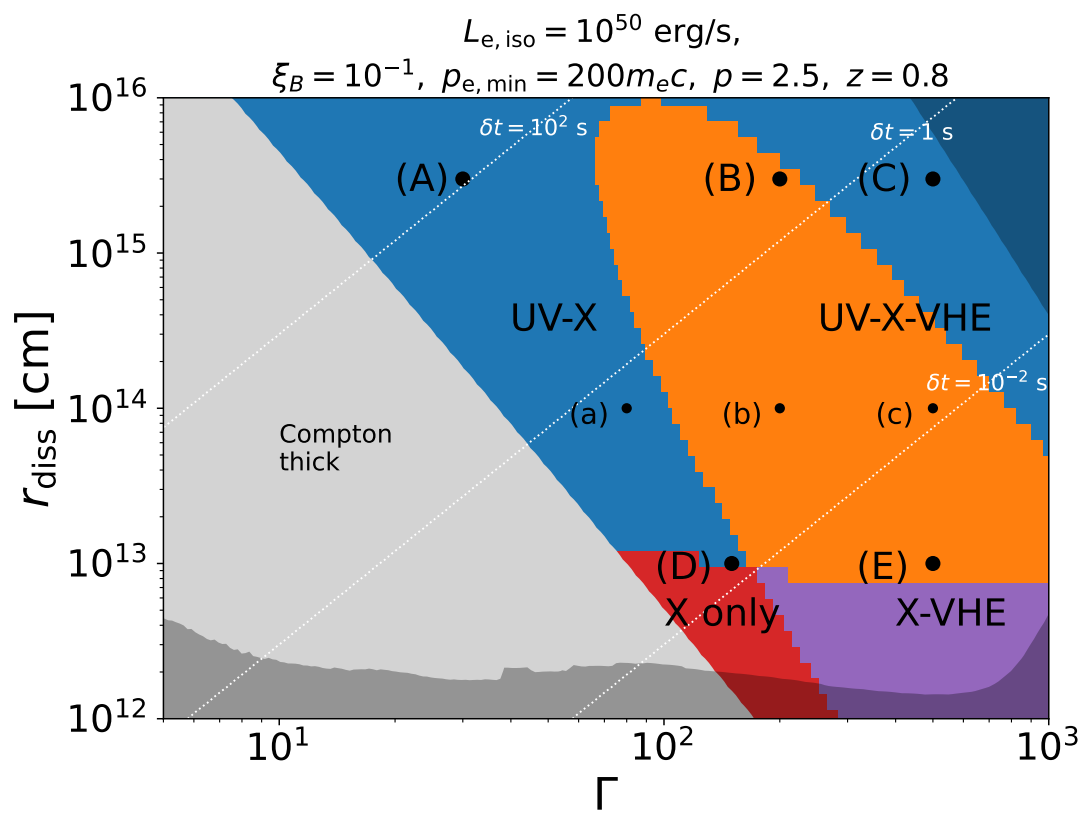


Figure 6. Same as Figure 2 but for $p = 2.5$.

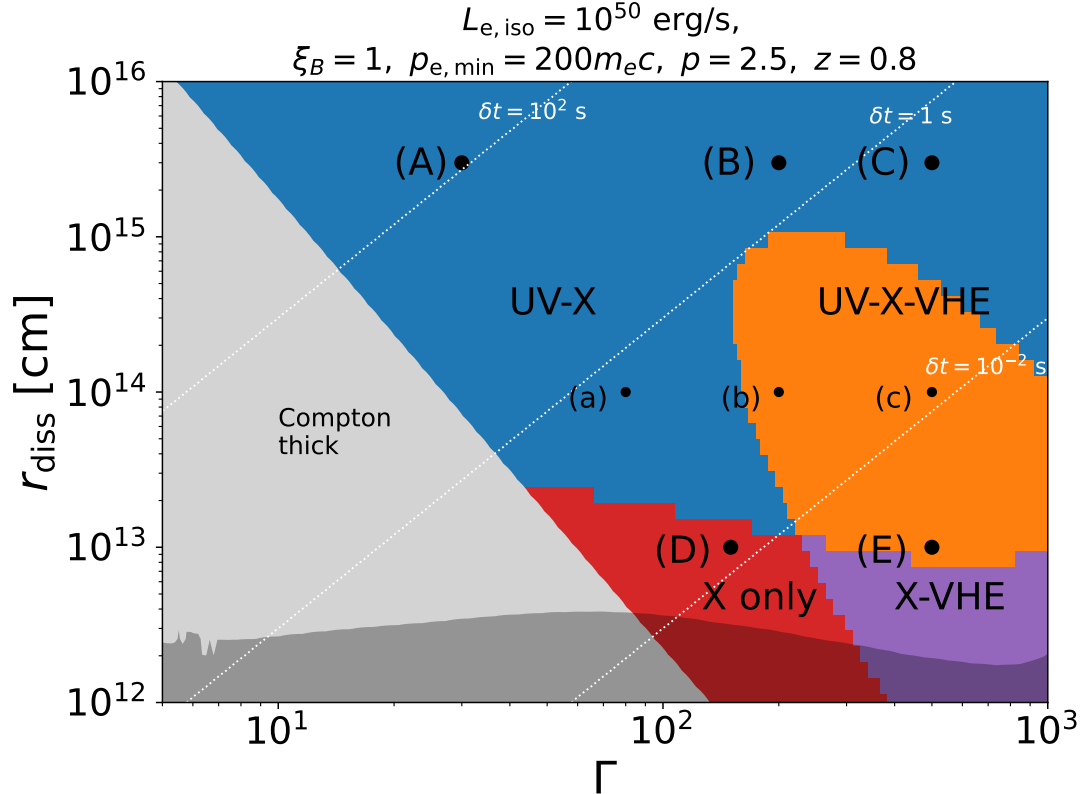


Figure 7. Same as Figure 2 but for $p = 2.5$ and $\xi_B = 10$.

Böttcher, M., & Dermer, C. D. 1998, ApJL, 499, L131, doi: [10.1086/311366](https://doi.org/10.1086/311366)

Bromberg, O., Nakar, E., Piran, T., & Sari, R. 2011, ApJ, 740, 100, doi: [10.1088/0004-637X/740/2/100](https://doi.org/10.1088/0004-637X/740/2/100)

Burrows, D. N., Romano, P., Falcone, A., et al. 2005a, Science, 309, 1833, doi: [10.1126/science.1116168](https://doi.org/10.1126/science.1116168)

Burrows, D. N., Hill, J. E., Nousek, J. A., et al. 2005b, SSRv, 120, 165, doi: [10.1007/s11214-005-5097-2](https://doi.org/10.1007/s11214-005-5097-2)

Cao, Z., della Volpe, D., Liu, S., et al. 2019, arXiv e-prints, arXiv:1905.02773, doi: [10.48550/arXiv.1905.02773](https://doi.org/10.48550/arXiv.1905.02773)

Cornejo Avila, B., Ashkar, H., Cerruti, M., et al. 2026, in 39th International Cosmic Ray Conference, 615

Dainotti, M. G., Willingale, R., Capozziello, S., Fabrizio Cardone, V., & Ostrowski, M. 2010, ApJL, 722, L215, doi: [10.1088/2041-8205/722/2/L215](https://doi.org/10.1088/2041-8205/722/2/L215)

Dermer, C. D., & Menon, G. 2009, High Energy Radiation from Black Holes: Gamma Rays, Cosmic Rays, and Neutrinos

Duque, R., Beniamini, P., Daigne, F., & Mochkovitch, R. 2022, MNRAS, 513, 951, doi: [10.1093/mnras/stac938](https://doi.org/10.1093/mnras/stac938)

Falcone, A. D., Burrows, D. N., Lazzati, D., et al. 2006, ApJ, 641, 1010, doi: [10.1086/500655](https://doi.org/10.1086/500655)

Falcone, A. D., Morris, D., Racusin, J., et al. 2007, ApJ, 671, 1921, doi: [10.1086/523296](https://doi.org/10.1086/523296)

Fan, Y. Z., & Wei, D. M. 2005, MNRAS, 364, L42, doi: [10.1111/j.1745-3933.2005.00102.x](https://doi.org/10.1111/j.1745-3933.2005.00102.x)

Fioretti, V., Ribeiro, D., Humensky, T. B., et al. 2019, in International Cosmic Ray Conference, Vol. 36, 36th International Cosmic Ray Conference (ICRC2019), 673, doi: [10.22323/1.358.0673](https://doi.org/10.22323/1.358.0673)

Fuschino, F., Campana, R., Labanti, C., et al. 2019, Nuclear Instruments and Methods in Physics Research A, 936, 199, doi: [10.1016/j.nima.2018.11.072](https://doi.org/10.1016/j.nima.2018.11.072)

Gao, W.-H., & Fan, Y.-Z. 2006, ChJAA, 6, 513, doi: [10.1088/1009-9271/6/5/01](https://doi.org/10.1088/1009-9271/6/5/01)

Gehrels, N., Chincarini, G., Giommi, P., et al. 2004, ApJ, 611, 1005, doi: [10.1086/422091](https://doi.org/10.1086/422091)

Ghisellini, G., Nardini, M., Ghirlanda, G., & Celotti, A. 2009, MNRAS, 393, 253, doi: [10.1111/j.1365-2966.2008.14214.x](https://doi.org/10.1111/j.1365-2966.2008.14214.x)

Gilmore, R. C., Somerville, R. S., Primack, J. R., & Domínguez, A. 2012, MNRAS, 422, 3189, doi: [10.1111/j.1365-2966.2012.20841.x](https://doi.org/10.1111/j.1365-2966.2012.20841.x)

Gompertz, B. P., O'Brien, P. T., & Wynn, G. A. 2014, MNRAS, 438, 240, doi: [10.1093/mnras/stt2165](https://doi.org/10.1093/mnras/stt2165)

Gompertz, B. P., O'Brien, P. T., Wynn, G. A., & Rowlinson, A. 2013, MNRAS, 431, 1745, doi: [10.1093/mnras/stt293](https://doi.org/10.1093/mnras/stt293)

Goodman, J. 1986, *ApJL*, 308, L47, doi: [10.1086/184741](https://doi.org/10.1086/184741)

Gottlieb, O., Bromberg, O., Singh, C. B., & Nakar, E. 2020, *MNRAS*, 498, 3320, doi: [10.1093/mnras/staa2567](https://doi.org/10.1093/mnras/staa2567)

Gottlieb, O., Nakar, E., & Bromberg, O. 2021, *MNRAS*, 500, 3511, doi: [10.1093/mnras/staa3501](https://doi.org/10.1093/mnras/staa3501)

Gotz, D., Adami, C., Basa, S., et al. 2014, in *Proceedings of Swift: 10 Years of Discovery (SWIFT 10*, 74, doi: [10.22323/1.233.0074](https://doi.org/10.22323/1.233.0074)

Hamidani, H., & Ioka, K. 2021, *MNRAS*, 500, 627, doi: [10.1093/mnras/staa3276](https://doi.org/10.1093/mnras/staa3276)

Hamidani, H., & Ioka, K. 2023, *MNRAS*, 520, 1111, doi: [10.1093/mnras/stad041](https://doi.org/10.1093/mnras/stad041)

Hao, J.-M., Cao, L., Lu, Y.-J., et al. 2020, *ApJS*, 248, 21, doi: [10.3847/1538-4365/ab88da](https://doi.org/10.3847/1538-4365/ab88da)

Hofmann, W., & Zanin, R. 2023, arXiv e-prints, arXiv:2305.12888, doi: [10.48550/arXiv.2305.12888](https://doi.org/10.48550/arXiv.2305.12888)

Inoue, S., Granot, J., O'Brien, P. T., et al. 2013, *Astroparticle Physics*, 43, 252, doi: [10.1016/j.astropartphys.2013.01.004](https://doi.org/10.1016/j.astropartphys.2013.01.004)

Ioka, K., Kobayashi, S., & Zhang, B. 2005, *ApJ*, 631, 429, doi: [10.1086/432567](https://doi.org/10.1086/432567)

Jin, Z.-P., Zhou, H., Wang, Y., et al. 2023, *Nature Astronomy*, 7, 1108, doi: [10.1038/s41550-023-02005-w](https://doi.org/10.1038/s41550-023-02005-w)

Kagawa, Y., Yonetoku, D., Sawano, T., et al. 2019, *ApJ*, 877, 147, doi: [10.3847/1538-4357/ab1bd6](https://doi.org/10.3847/1538-4357/ab1bd6)

Kagawa, Y., Yonetoku, D., Sawano, T., et al. 2015, *ApJ*, 811, 4, doi: [10.1088/0004-637X/811/1/4](https://doi.org/10.1088/0004-637X/811/1/4)

Kaneko, Y., Bostancı, Z. F., Göğüş, E., & Lin, L. 2015, *MNRAS*, 452, 824, doi: [10.1093/mnras/stv1286](https://doi.org/10.1093/mnras/stv1286)

Kimura, S. S., Murase, K., Ioka, K., et al. 2019, *ApJL*, 887, L16, doi: [10.3847/2041-8213/ab59e1](https://doi.org/10.3847/2041-8213/ab59e1)

Kisaka, S., & Ioka, K. 2015, *ApJL*, 804, L16, doi: [10.1088/2041-8205/804/1/L16](https://doi.org/10.1088/2041-8205/804/1/L16)

Kisaka, S., Ioka, K., & Sakamoto, T. 2017, *ApJ*, 846, 142, doi: [10.3847/1538-4357/aa8775](https://doi.org/10.3847/1538-4357/aa8775)

Kouveliotou, C., Meegan, C. A., Fishman, G. J., et al. 1993, *ApJL*, 413, L101, doi: [10.1086/186969](https://doi.org/10.1086/186969)

Kumar, P., Narayan, R., & Johnson, J. L. 2008, *MNRAS*, 388, 1729, doi: [10.1111/j.1365-2966.2008.13493.x](https://doi.org/10.1111/j.1365-2966.2008.13493.x)

Lei, W.-H., Zhang, B., Wu, X.-F., & Liang, E.-W. 2017, *ApJ*, 849, 47, doi: [10.3847/1538-4357/aa9074](https://doi.org/10.3847/1538-4357/aa9074)

Liang, E. W., Zhang, B., O'Brien, P. T., et al. 2006, *ApJ*, 646, 351, doi: [10.1086/504684](https://doi.org/10.1086/504684)

Lien, A., Sakamoto, T., Barthelmy, S. D., et al. 2016, *ApJ*, 829, 7, doi: [10.3847/0004-637X/829/1/7](https://doi.org/10.3847/0004-637X/829/1/7)

Liu, C., & Mao, J. 2019a, *ApJ*, 884, 59, doi: [10.3847/1538-4357/ab3e75](https://doi.org/10.3847/1538-4357/ab3e75)

Liu, C., & Mao, J. 2019b, *ApJ*, 884, 59, doi: [10.3847/1538-4357/ab3e75](https://doi.org/10.3847/1538-4357/ab3e75)

Lundman, C., & Beloborodov, A. M. 2019a, *ApJ*, 879, 83, doi: [10.3847/1538-4357/ab229f](https://doi.org/10.3847/1538-4357/ab229f)

Lundman, C., & Beloborodov, A. M. 2019b, *ApJ*, 879, 83, doi: [10.3847/1538-4357/ab229f](https://doi.org/10.3847/1538-4357/ab229f)

Lyons, N., O'Brien, P. T., Zhang, B., et al. 2010, *MNRAS*, 402, 705, doi: [10.1111/j.1365-2966.2009.15538.x](https://doi.org/10.1111/j.1365-2966.2009.15538.x)

Matsui, R., Kimura, S. S., & Hamidani, H. 2024, *ApJ*, 974, 185, doi: [10.3847/1538-4357/ad6f09](https://doi.org/10.3847/1538-4357/ad6f09)

Matsui, R., Kimura, S. S., Toma, K., & Murase, K. 2023, *ApJ*, 950, 190, doi: [10.3847/1538-4357/acd004](https://doi.org/10.3847/1538-4357/acd004)

Matsumoto, T., Kimura, S. S., Murase, K., & Mészáros, P. 2020, *MNRAS*, 493, 783, doi: [10.1093/mnras/staa305](https://doi.org/10.1093/mnras/staa305)

Matzner, C. D. 2003, *MNRAS*, 345, 575, doi: [10.1046/j.1365-8711.2003.06969.x](https://doi.org/10.1046/j.1365-8711.2003.06969.x)

Mei, A., Banerjee, B., Oganesyan, G., et al. 2022, *Nature*, 612, 236, doi: [10.1038/s41586-022-05404-7](https://doi.org/10.1038/s41586-022-05404-7)

Mészáros, P., & Rees, M. J. 2001, *ApJL*, 556, L37, doi: [10.1086/322934](https://doi.org/10.1086/322934)

Metzger, B. D., Quataert, E., & Thompson, T. A. 2008, *MNRAS*, 385, 1455, doi: [10.1111/j.1365-2968.2008.12923.x](https://doi.org/10.1111/j.1365-2968.2008.12923.x)

Murase, K. 2008, *Phys. Rev. D*, 78, 101302, doi: [10.1103/PhysRevD.78.101302](https://doi.org/10.1103/PhysRevD.78.101302)

Murase, K., Asano, K., Terasawa, T., & Meszaros, P. 2012, *Astrophys. J.*, 746, 164, doi: [10.1088/0004-637X/746/2/164](https://doi.org/10.1088/0004-637X/746/2/164)

Murase, K., & Beacom, J. F. 2010, *Phys. Rev. D*, 82, 043008, doi: [10.1103/PhysRevD.82.043008](https://doi.org/10.1103/PhysRevD.82.043008)

Murase, K., & Nagataki, S. 2006, *PhRvL*, 97, 051101, doi: [10.1103/PhysRevLett.97.051101](https://doi.org/10.1103/PhysRevLett.97.051101)

Murase, K., Toma, K., Yamazaki, R., & Mészáros, P. 2011, *ApJ*, 732, 77, doi: [10.1088/0004-637X/732/2/77](https://doi.org/10.1088/0004-637X/732/2/77)

Nakar, E., & Piran, T. 2017, *ApJ*, 834, 28, doi: [10.3847/1538-4357/834/1/28](https://doi.org/10.3847/1538-4357/834/1/28)

Norris, J. P., & Bonnell, J. T. 2006, *ApJ*, 643, 266, doi: [10.1086/502796](https://doi.org/10.1086/502796)

ousek, J. A., Kouveliotou, C., Grupe, D., et al. 2006, *ApJ*, 642, 389, doi: [10.1086/500724](https://doi.org/10.1086/500724)

Paczynski, B. 1986, *ApJL*, 308, L43, doi: [10.1086/184740](https://doi.org/10.1086/184740)

Peng, F.-K., Liang, E.-W., Wang, X.-Y., et al. 2014, *ApJ*, 795, 155, doi: [10.1088/0004-637X/795/2/155](https://doi.org/10.1088/0004-637X/795/2/155)

Perna, R., Armitage, P. J., & Zhang, B. 2006, *ApJL*, 636, L29, doi: [10.1086/499775](https://doi.org/10.1086/499775)

Piro, L., De Pasquale, M., Soffitta, P., et al. 2005, *ApJ*, 623, 314, doi: [10.1086/428377](https://doi.org/10.1086/428377)

Racusin, J. L., Karpov, S. V., Sokolowski, M., et al. 2008, *Nature*, 455, 183, doi: [10.1038/nature07270](https://doi.org/10.1038/nature07270)

Rees, M. J., & Meszaros, P. 1994, *ApJL*, 430, L93, doi: [10.1086/187446](https://doi.org/10.1086/187446)

Rees, M. J., & Mészáros, P. 2005, ApJ, 628, 847, doi: [10.1086/430818](https://doi.org/10.1086/430818)

Ribeiro, D. 2023, in The Sixteenth Marcel Grossmann Meeting. On Recent Developments in Theoretical and Experimental General Relativity, Astrophysics, and Relativistic Field Theories, ed. R. Ruffino & G. Vereshchagin, 3017–3029, doi: [10.1142/9789811269776.0244](https://doi.org/10.1142/9789811269776.0244)

Rowlinson, A., O'Brien, P. T., Metzger, B. D., Tanvir, N. R., & Levan, A. J. 2013, MNRAS, 430, 1061, doi: [10.1093/mnras/sts683](https://doi.org/10.1093/mnras/sts683)

Sakamoto, T., Barthelmy, S. D., Baumgartner, W. H., et al. 2011, ApJS, 195, 2, doi: [10.1088/0067-0049/195/1/2](https://doi.org/10.1088/0067-0049/195/1/2)

Schmidt, W. K. H. 1978, Nature, 271, 525, doi: [10.1038/271525a0](https://doi.org/10.1038/271525a0)

Swenson, C. A., & Roming, P. W. A. 2014, ApJ, 788, 30, doi: [10.1088/0004-637X/788/1/30](https://doi.org/10.1088/0004-637X/788/1/30)

Swenson, C. A., Roming, P. W. A., De Pasquale, M., & Oates, S. R. 2013, ApJ, 774, 2, doi: [10.1088/0004-637X/774/1/2](https://doi.org/10.1088/0004-637X/774/1/2)

Toma, K., Wu, X.-F., & Mészáros, P. 2009, ApJ, 707, 1404, doi: [10.1088/0004-637X/707/2/1404](https://doi.org/10.1088/0004-637X/707/2/1404)

Troja, E., Piro, L., Vasileiou, V., et al. 2015, ApJ, 803, 10, doi: [10.1088/0004-637X/803/1/10](https://doi.org/10.1088/0004-637X/803/1/10)

Vetri, M. 1995, ApJ, 453, 883, doi: [10.1086/176448](https://doi.org/10.1086/176448)

Vurm, I., & Poutanen, J. 2009, ApJ, 698, 293, doi: [10.1088/0004-637X/698/1/293](https://doi.org/10.1088/0004-637X/698/1/293)

Waxman, E. 1995, PhRvL, 75, 386, doi: [10.1103/PhysRevLett.75.386](https://doi.org/10.1103/PhysRevLett.75.386)

Waxman, E., & Bahcall, J. 1997, PhRvL, 78, 2292, doi: [10.1103/PhysRevLett.78.2292](https://doi.org/10.1103/PhysRevLett.78.2292)

Weekes, T. C., Badran, H., Biller, S. D., et al. 2002, Astroparticle Physics, 17, 221, doi: [10.1016/S0927-6505\(01\)00152-9](https://doi.org/10.1016/S0927-6505(01)00152-9)

Werner, N., Řípa, J., Pál, A., et al. 2018, in Society of Photo-Optical Instrumentation Engineers (SPIE) Conference Series, Vol. 10699, Space Telescopes and Instrumentation 2018: Ultraviolet to Gamma Ray, ed. J.-W. A. den Herder, S. Nikzad, & K. Nakazawa, 106992P, doi: [10.1117/12.2313764](https://doi.org/10.1117/12.2313764)

Yi, S.-X., Wu, X.-F., Wang, F.-Y., & Dai, Z.-G. 2015, ApJ, 807, 92, doi: [10.1088/0004-637X/807/1/92](https://doi.org/10.1088/0004-637X/807/1/92)

Yi, S.-X., Xi, S.-Q., Yu, H., et al. 2016, ApJS, 224, 20, doi: [10.3847/0067-0049/224/2/20](https://doi.org/10.3847/0067-0049/224/2/20)

Yi, S.-X., Yu, H., Wang, F. Y., & Dai, Z.-G. 2017, ApJ, 844, 79, doi: [10.3847/1538-4357/aa7b7b](https://doi.org/10.3847/1538-4357/aa7b7b)

Zhang, B. 2019, The physics of gamma-ray bursts

Zhang, B., Fan, Y. Z., Dyks, J., et al. 2006a, ApJ, 642, 354, doi: [10.1086/500723](https://doi.org/10.1086/500723)

Zhang, B., Fan, Y. Z., Dyks, J., et al. 2006b, ApJ, 642, 354, doi: [10.1086/500723](https://doi.org/10.1086/500723)

Zhang, B., & Kumar, P. 2013, PhRvL, 110, 121101, doi: [10.1103/PhysRevLett.110.121101](https://doi.org/10.1103/PhysRevLett.110.121101)

Zhang, B., & Yan, H. 2011, ApJ, 726, 90, doi: [10.1088/0004-637X/726/2/90](https://doi.org/10.1088/0004-637X/726/2/90)

Zhang, B. T., & Murase, K. 2023, Mon. Not. Roy. Astron. Soc., 524, 76, doi: [10.1093/mnras/stad1829](https://doi.org/10.1093/mnras/stad1829)

Zhang, B. T., Murase, K., Yuan, C., Kimura, S. S., & Mészáros, P. 2021, ApJL, 908, L36, doi: [10.3847/2041-8213/abe0b0](https://doi.org/10.3847/2041-8213/abe0b0)

Zhou, Z.-M., Chen, L.-J., Li, R.-Q., et al. 2025, ApJ, 984, 81, doi: [10.3847/1538-4357/adc45c](https://doi.org/10.3847/1538-4357/adc45c)

Zrake, J., Beloborodov, A. M., & Lundman, C. 2019, ApJ, 885, 30, doi: [10.3847/1538-4357/ab364b](https://doi.org/10.3847/1538-4357/ab364b)